High resolution near-IR spectroscopy of FGK stars

Daniel Thaagaard Andreasen

March 10, 2017

To Linnea, Henriette, and Rico
For always supporting me

Contents

Abstracts

List of Figures

List of Tables

Chapter 1

Introduction

Effective temperature (T_{eff}), surface gravity ($\log g$), and metallicity ([M/H], where iron is normally used as a proxy) are fundamental atmospheric parameters necessary to characterise a single star, and to determine other indirectly fundamental parameters such as mass, radius, and age from stellar evolution models (see e.g. Baraffe et al., 2015; Dotter et al., 2008; Girardi et al., 2000). Precise and accurate stellar parameters are also essential in exoplanet searches. Planetary radius and mass are mainly found from transit lightcurve analysis and radial velocity analysis, respectively. The determination of the mass of the planet implies a knowledge of the stellar mass, while the measurement of the radius of the planet is dependent on our capability to derive the radius of the star (see e.g. Ammler-von Eiff et al., 2009; Torres et al., 2012, 2008).

The derivation of precise stellar atmospheric parameters is not a simple task. Different approaches often lead to discrepant results (see e.g. Lebzelter et al., 2012; Santos et al., 2013; Torres et al., 2010). Interferometry is usually considered an accurate method for deriving stellar radii (see e.g. Boyajian et al., 2012); however, it is only applicable for bright nearby stars. Asteroseismology, on the other hand, reveals the inner stellar structure by observing the stellar pulsations at the surface. From asteroseismology it is possible to measure the surface gravity and mean density, and therefore to calculate mass and radius with high precision (see e.g. Kjeldsen and Bedding, 1995). However, for stars on the main sequence asteroseismic methods can typically only be applied to FG stars, since the oscillation modes of K and M dwarfs are likely too weak to be detected even with high precision spectroscopy or photometry. Moreover, the effective temperature is needed when applying asteroseismology in order to obtain the surface gravity and the mean density.

A crucial parameter for the indirect determination of stellar bulk properties is the T_{eff}. In that respect, the infrared flux method (IRFM) has proven to be reliable for FGK dwarf and subgiant stars. For higher accuracy the IRFM needs a priori knowledge of the bolometric flux, reddening, surface gravity, and stellar metallicity (Blackwell and Shallis, 1977; Casagrande et al., 2010; Ramírez and Meléndez, 2005).

Finally, the use of high resolution spectroscopy along with stellar atmospheric models is an extensively tested method that allows the derivation of the fundamental parameters of a star (see e.g. Santos et al., 2013; Valenti and Fischer, 2005). The procedure depends on the quality of the spectra, their resolution, and wavelength region. A fit to the overall spectrum can be applied for all spectral resolutions, but are often time consuming (see e.g. Recio-Blanco et al., 2006; Tsantaki et al., 2014). For resolutions higher than $\lambda/\Delta\lambda \sim 20\,000$ we can apply the equivalent width (EW) method (see e.g. Andreasen et al., 2017; Tsantaki et al., 2013, for details). However, while the latter approach is often faster than the synthetic fitting, it requires higher quality spectra, and the star to be slow rotating (below 10 km/s to 15 km/s).

Standard procedures are often used to derive stellar atmospheric parameters from high quality spectra in the optical (see e.g. Sousa et al., 2008; Valenti and Fischer, 2005). With the advancement of high resolution near-infrared (NIR) instruments, we will now be able to use a similar technique to that used in the optical part of the spectrum (see e.g. Bensby et al., 2014; Meléndez and Barbuy, 1999; Mucciarelli et al., 2013; Sousa et al., 2008; Tsantaki et al., 2013). At the moment, the GIANO spectrograph installed at *Telescopio Nazionale Galileo* (TNG) is already available (Origlia et al., 2014), as is the *infrared Doppler instrument* (IRD) installed at the Subaru telescope (Kotani et al., 2014), *Calar Alto high-Resolution search for M dwarfs with Exoearths with Near-infrared and optical Échelle Spectrographs* (CARMENES) for the 3.5 m telescope at Calar Alto Observatory (Quirrenbach et al., 2014), and iShell at the *InfraRed Telescope Facility* (Rayner et al., 2012, 2016). Three new spectrographs are planned for the near future: 1) The *CRyogenic InfraRed Echelle Spectrograph Upgrade Project* (CRIRES+) at the *Very Large Telescope* (VLT) (Follert et al., 2014) with expected first light in 2017, 2) *un SpectroPolarimètre Infra-Rouge A Near-InfraRed Spectropolarimeter* (SPIRou) at *The Canada-France-Hawaii Telescope* (CFHT) (Artigau et al., 2014; Delfosse et al., 2013) with expected first light in 2017 as well, and 3) *Near Infrared Planet Searcher* NIRPS at the ESO 3.6m telescope in La Silla (Conod et al., 2016). The spectral resolutions for these spectrographs range between 50 000 and 100 000.

With the advance of the next generation NIR spectrographs, we are still preparing the data analysis of stellar spectra, in particular how to get reliable atmospheric parameters (see e.g. Andreasen et al., 2016; Lindgren et al., 2016; Önehag et al., 2012). The analysis of stellar spectra is well understood for FGK stars in the optical part of the spectrum, however some work still needs to be done for the NIR part.

We continue our series of studies to explore the use of the NIR domain to derive stellar parameters for FGK and M stars. In particular, here we analyse the atlas of Arcturus and the spectrum of 10 Leo. For the analysis we use the iron line list presented in Andreasen et al. (2016) (referred to as Paper I). In Paper I we successfully tested our method on a slightly hotter star than the Sun, while in this work we aim to test the method on cooler stars. The strength of the NIR domain over the optical becomes clear when we move towards the cooler stars. Here we see less continuum depression and line blending due to in particular molecular features. Moreover, the cooler stars emit more light in the NIR domain than the optical, and with the lightest stars being intrinsically faint, we thus obtain the majority of the flux here.

1.1 Planet host stars

With the present diversity of exoplanets ot becomes increasingly important to get an accurate and precise characterization of the planets in order to study them in samples and on an individual level. An accurate and precise characterization can give us an idea wether the planet is rocky, composed of water or gaseous.

1.2 Atmospheric parameters

CHAPTER 2

THEORY

To encompass all theory regarding stellar structure, evolution, and their atmosphere is far beyond the scope of this thesis. Rather the theory needed is presented below with highlights on the most important aspects.

2.1 Stellar structure

The structure of a non-rotating spherical stars can be described by five rather simple differential equations (see e.g. Kippenhahn and Weigert, 1994) presented below:

1. **Equation of Continuity**

   Relation between the mass, m, the density, ρ, at a symmetric shell at radius r

$$\boxed{\frac{\partial r}{\partial m} = \frac{1}{4\pi r^2 \rho}.} \tag{2.1}$$

2. **Equation of Hydrostatic Equilibrium**

   The equation of hydrostatic equilibrium shows how a star in equilibrium is balanced between two forces. The inward force from gravity and the outward force from pressure, P,

$$\boxed{\frac{\partial P}{\partial m} = -\frac{Gm}{4\pi r^4}.} \tag{2.2}$$

When working with asteroseismology a time dependent perturbation to this equation is added (see e.g. Aerts et al., 2010, for a thorough discussion). However, this term is neglected here.

3. **Equation of Energy Conservation**

   The equation of energy conservation shows how the energy is produced and lost throughout the star.

$$\boxed{\frac{\partial l}{\partial m} = \varepsilon - \varepsilon_{\nu} + \varepsilon_{g},} \tag{2.3}$$

   where ε is the energy production in the centre of the star, ε_{ν} is the energy lost by neutrinos which is always positive, ε_{g} is a source function of time-dependent terms, and l is the luminosity at m. ε_{g} comes from the fact that non-stationary shells can change its internal energy, and thus exchange mechanical energy with neighbouring shells.

4. **Equation of Energy Transport**

   Energy transportation throughout the star is described with the following equation

$$\boxed{\frac{\partial T}{\partial m} = -\frac{GmT}{4\pi r^4 P}\nabla_{\mathrm{rad}},} \tag{2.4}$$

   where ∇_{rad} is the radiative temperature gradient, and T is the temperature. The value of the temperature gradient compared to the radiative temperature gradient tells if the energy is transported by convection or radiation. In our Sun the outer layer are convective while the inner layer are radiative.

5. **Equation of Chemical Composition**

   In this last equation we see the evolution of an element, X_i, when it reacts with other elements with reaction rates r_{ji} and r_{ik}

$$\boxed{\frac{\partial X_i}{\partial t} = \frac{m_i}{\rho}\left(\sum_j r_{ji} - \sum_k r_{ik}\right).} \tag{2.5}$$

   Note that this is the only time-dependent equation of the five presented.

These five fundamental equations are implemented in stellar evolutionary codes, which we will use in later chapters. The many different codes that exist take other things into account, e.g the star can rotate, and it may not always be in hydrostatic equilibrium (this is important if we want our star to pulsate). For simplicity we have only presented time-dependence in the Equation of Chemical Composition since timescales of rotation, pulsations, and activity are much shorter than the long timescale found in chemical composition changes.

2.2 Stellar atmosphere

Much of this Section is inspired by Gray (2005). While all the figures here were made by the author of this thesis, most of them can be found in Gray (2005) as well.

Stellar atmospheres are rather complicated. This is where the light produced in the interior of the stars are released. However, the atmosphere of a star is not transparent to all light, and some of the light is absorbed in the atmosphere and later emitted in a random direction. The different elements in the atmosphere is the reason for absorbing light at specific wavelength. The strength of the absorption depends on the physical conditions in the atmosphere, the effective temperature (T_{eff}), the pressure/gravity ($\log g$), the overall metallicity ([Fe /H]), the specific abundance of a given element if different from the overall metallicity (A), and the atomic characteristics of the transition coursing the absorption line.

It is important to know the fraction of atoms excited to the nth energy level, N_n. This fraction is proportional to the statistical weight g_n and the Boltzmann factor and is described as:

$$\boxed{\frac{N_n}{N} = \frac{g_n}{u(T)} 10^{-\theta\chi_n}} \qquad \text{Boltzmann}$$

This equation is also called the Boltzmann equation. Here N is the total number of atoms per unit volume, $u(T) = \Sigma g_i e^{-\chi_i/kT}$ is the partition function, k is Boltzmann's constant, T is the temperature, and χ_n is the excitation potential for the lower energy level.

While atoms can get excited following Boltzmann's equation above, they can also get ionised. The ionisation for a collision dominated gas (which is a good approximation for FGKM stars), the ratio of neutral atoms to single ionised atoms is described by the Saha equation:

$$\boxed{\frac{N_1}{N_0} P_e = \frac{(2\pi m_e)^{3/2}(kT)^{5/2}}{h^3} \frac{2u_1(T)}{u_0(T)} e^{-I/kT}} \qquad \text{Saha}$$

here m_e is the electron mass, h is Planck's constant, and I is the ionisation potential of the ion.

The atomic lines are characterised by few quantum mechanical descriptors.

- The wavelength describes between which energy levels there is a transition, i.e. at which wavelength the light is absorbed.
- The ionisation state, i.e. is it a atom element absorbing or a ionised atom.
- The excitation potential. This gives an idea how deep in the atmosphere a line is formed. If χ is high, then higher temperatures (i.e. higher random motion and more collisions between the atoms) is required for forming the absorption line. These higher temperatures are found deeper in the atmosphere.
- The oscillator strength, $\log gf$, is related to the atomic transition probability.
- The damping coefficients, is a natural damping (also known as radiation damping) caused by the uncertainty of lifetime in an energy level according to Heisenberg's uncertainty principle. This is related to a uncertainty in the energy level and thus a natural broadening is introduced.

2.2.1 The equivalent width

Measuring the equivalent width (EW) of spectral lines are important for some analysis of stellar spectra. The EW is a measure of the strength of the line, and dependent on the atmospheric conditions in where the spectral line is formed, such as T_{eff}, $\log g$, [Fe /H], and ξ_{micro}.

The EW is mathematically described as integrating over the entire line, and assign this area to a rectangle from 0 to the continuum flux (F_c) with the width, EW. This is illustrated in Figure 2.1 on the facing page and the equation below:

$$EW = \int_0^\infty \frac{F_c - F(\lambda)}{F_c} d\lambda, \tag{2.6}$$

where λ is the wavelength. This is integral is assuming there is only one single line, hence the integral is over all wavelength. In practice the integral is calculated in small windows around a spectral line. See Section 2.3.2 on page 14 for more details on how this is performed in practice. The unit of the EW is the same as the wavelength used. Throughout this thesis we will use Ångström (1Å= 0.1 nm) for the wavelength, and mÅ for the EW.

2.2.1.1 Temperature dependence

As mentioned above the EW depends on the atmospheric parameters. The dependence on T_{eff} is the strongest dependence. At low T_{eff} neutral elements, say Fe I, are the strongest lines as the number of ionised atoms are too small to contribute significantly to the EW. This is the result the Saha equation. As

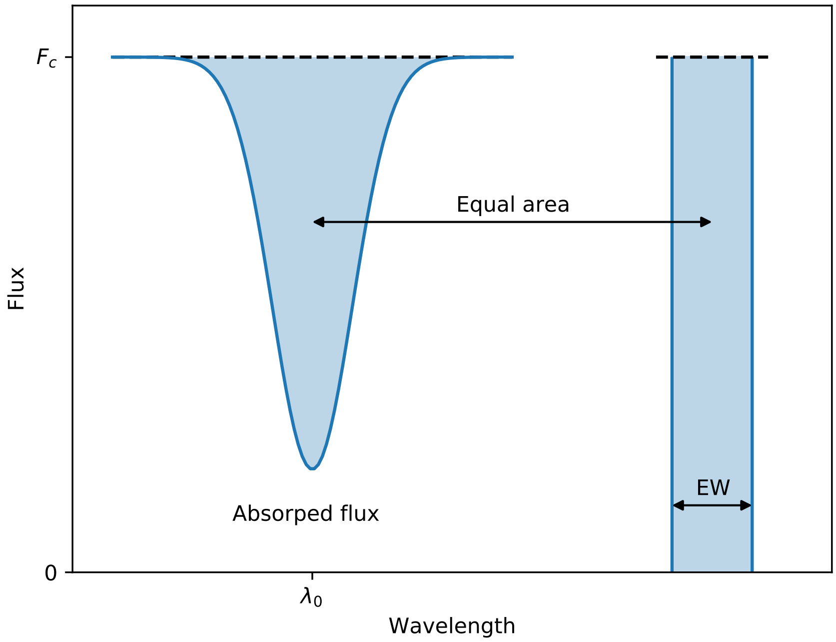

Figure 2.1: *An absorption line centred at λ_0 normalised at the flux level F_c. The area of the absorption line to the left is equal to the blue shaded area in the rectangle to the right with width EW.*

T_{eff} increases Fe I is converted into ionised Fe II. Slowly, as the number of Fe I decreases so does the EW, and likewise as the number of Fe II increases so does the EW. This goes on until second ionised atoms, Fe III, are formed and the same situation arise again. This is illustrated in Figure 2.2 on the following page where the EW of two iron lines, one neutral and one ionised, are plotted against T_{eff}. These two lines have similar EW in the Sun: 46.2 mÅ and 53.9 mÅ for the Fe I and Fe II line respectively.

2.2.1.2 Pressure dependence

Pressure dependence in the stellar atmosphere can be related to the gravity dependence. There are many ways to measure the pressure, and thus the gravity which is what is ultimately the goal with the measurement of $\log g$. Below are listed some of the most common methods to measure $\log g$ from spectroscopy.

- Continuum: The Balmer jump is the only continuum feature sensitive enough to estimate the $\log g$.

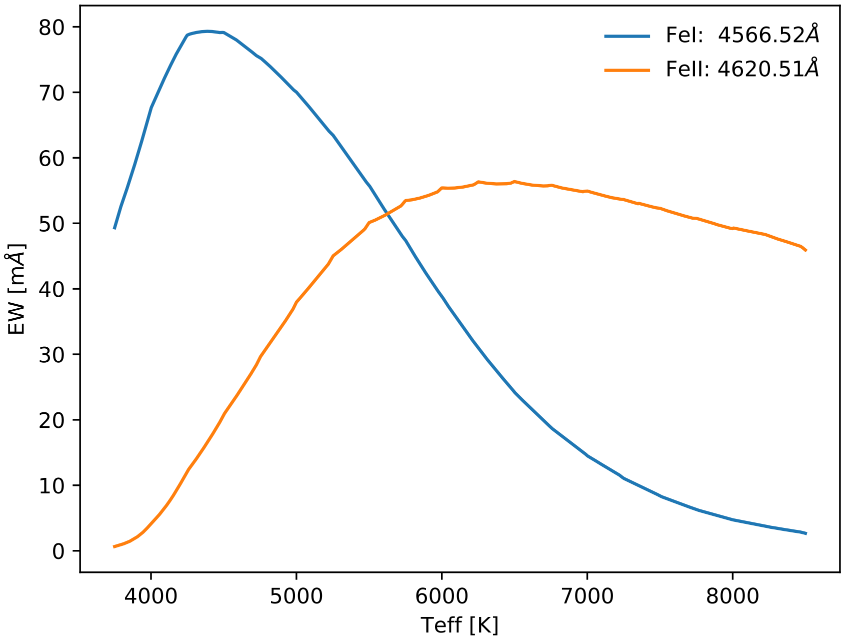

Figure 2.2: *The EW for a* Fe I *and* Fe II *line with increasing $T_{\rm eff}$. The two lines have similar EW in the Sun and are found in the optical part of the spectrum.*

- Hydrogen lines: Hydrogen profiles are pressure sensitive and can therefore be used to estimate $\log g$. However, the gravity dependence rapidly diminishes for temperatures above 10 000 K.

- Other strong lines: There exists other strong lines with pressure-broadened wings such as the Ca II H and K lines. These are better for cooler stars than the hydrogen lines described above.

- Weak lines: By comparing two stages of ionisation for the same element it is possible to obtain $\log g$ using weaker or modestly strong lines.

In this thesis weak lines are used to measure $\log g$. More specifically a comparison between Fe I and Fe II lines are used. For FGK stars, as the atmosphere contracts (i.e. $\log g$ increases) the pressure likewise increases, which in turn means that both the gas pressure, P_g, and electron pressure, P_e, increases. Since hydrogen is the main electron contributor, but not fully ionised for these stars, the electron pressure is much smaller that the gas pressure. The gas pressure follow a simply empirical approximation with gravity:

$$P_g \simeq \text{constant}\, g^{2/3}, \tag{2.7}$$

where g is the gravity.

NEED TO WRITE MORE HERE...

In Figure 2.3 is shown how the Fe II line used previously change with $\log g$. The curve of growth is shown in the upper panel, while a synthetic spectrum for each $\log g$ is presented in the lower left panel. It is clear that the ionised line is sensitive to $\log g$ as shown in the lower right panel, where the correlation between the abundance and $\log g$ is 0.40. This is expected as can be seen in Gray (2005, Table 16.1). There is used $\delta \log A / \delta \log g$ as an indicator, and for neutral elements the correlation is much weaker. It is important to note that the correlation does change with T_{eff} and the element used.

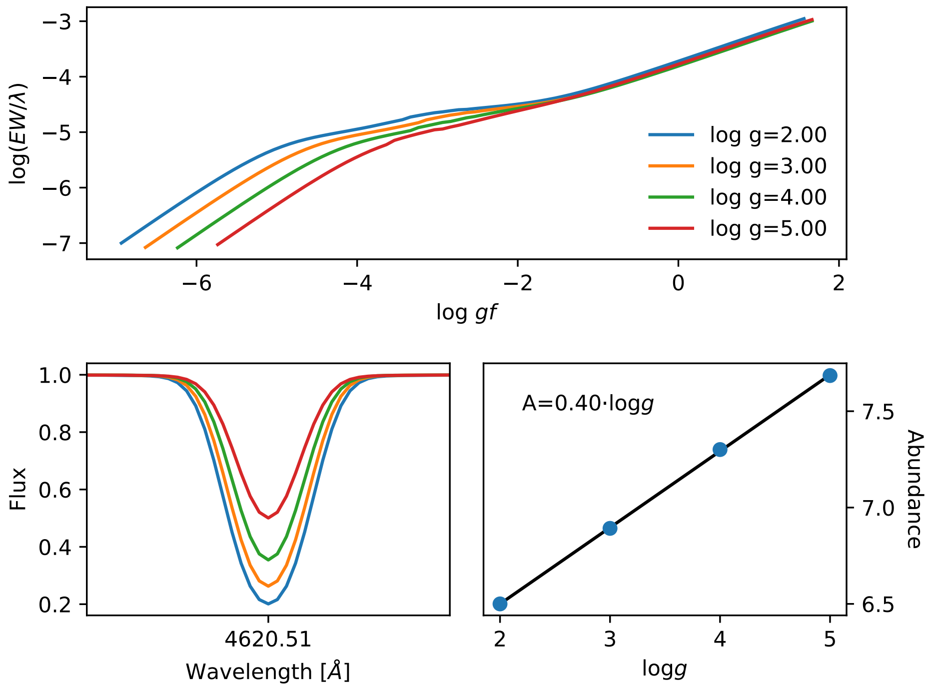

Figure 2.3: Upper panel: *Curve of growth for same* Fe II *used in Figure 2.2 on the preceding page for four different* $\log g$ *values. Here it is the weak lines mostly affected by the change in* $\log g$. Lower left panel: *Synthetic spectra of the same line. The colour scale is the same.* Lower right: *The abundance for the line at different* $\log g$. *A strong correlation (0.40) is seen.*

2.2.1.3 Abundance dependence

The abundance of a given element obviously has an effect on the EW. The more abundant an element is, the more photons can be absorbed thus increasing the EW. However, the relationship is not strictly linear. For weak lines (GIVE RANGE) EW is approximately linear with the abundance, however it reach a plateau where the core of the line saturates. In this regime the EW only increases slowly, until the absorption "spills" into the wings and the increase is again linear. However, for these strong lines the profile is no longer Gaussian. The curve of growth for the same Fe I line used in Figure 2.2 on page 10 is shown in Figure 2.4. Instead of EW it is common to use the reduced EW, $\log(EW/\lambda)$[1], which we will use more later. Instead of the abundance of a line, the oscillator strength, $\log gf$, is used.

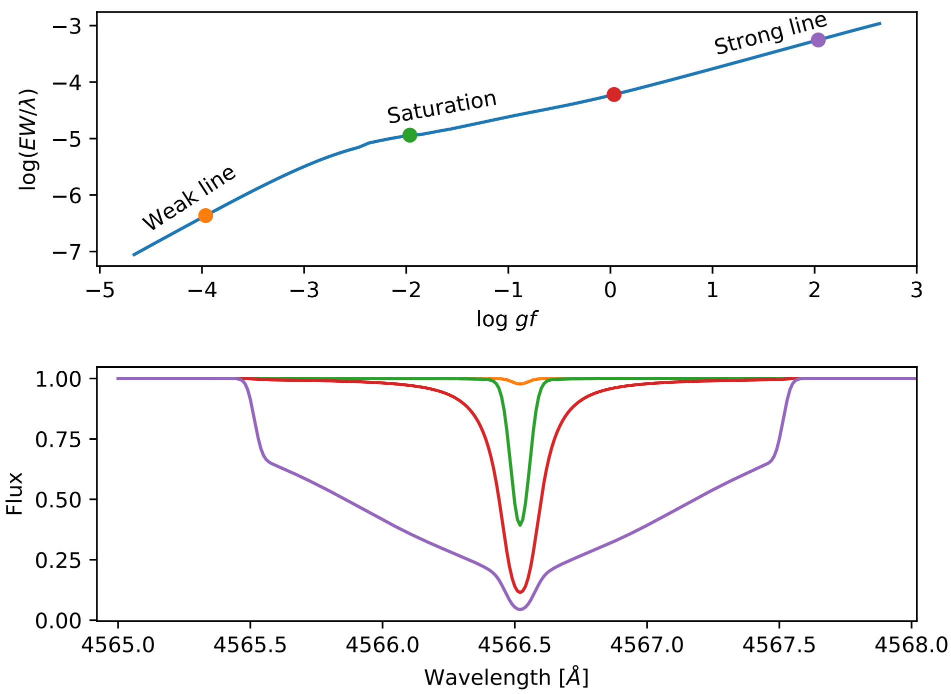

Figure 2.4: Upper panel: *Curve of growth of the same* Fe I *line as used in Figure 2.2 on page 10. Four points are marked which is shown in the* lower panel *as a synthetic spectral line. The RW (proxy for EW) is clearly increasing with* $\log gf$ *(proxy for abundance).*

[1] The reduced EW is useful since it normalises Doppler-dependent phenomena, such as microturbulence and thermal broadening.

2.2.1.4 Microturbulence

Small-scale motion, that is motion of material at length scales small compared to the unit optical depth, are called microturbulence, $\xi_{\rm micro}$. This is not to be confused with macroturbulence, which is motion of material at scales larger than the unit optical depth. The latter is associated with granulation and will not be discussed further in this thesis. $\xi_{\rm micro}$ comes into play when looking at the curve of growth for saturated lines (i.e. between green and red points in Figure 2.4 on the facing page). If no $\xi_{\rm micro}$ is assumed, then the measured abundance is higher than predicted by models based on thermal and damping broadening alone. In Figure 2.5 is shown three curves of growth with $\xi_{\rm micro} = 0.5\,{\rm km/s}, 2.5\,{\rm km/s}, 5.0\,{\rm km/s}$. As $\xi_{\rm micro}$ increases, so does the EW and hence the abundance.

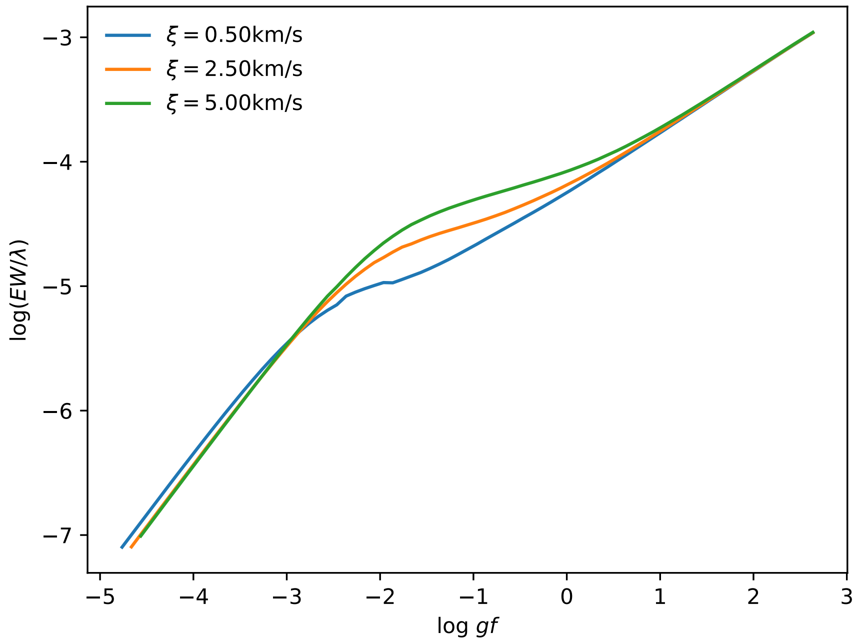

Figure 2.5: *Curve of growth for three different values of $\xi_{\rm micro}$. The EW is increasing with increasing $\xi_{\rm micro}$.*

The broadening of an absorption line measured by the shift in wavelength, $\Delta\lambda$, when $\xi_{\rm micro}$ is included is defined as:

$$\Delta\lambda = \frac{\lambda_0}{c}\sqrt{\frac{2kT}{m} + \xi_{\rm micro}^2}, \tag{2.8}$$

where c is the speed of light, λ_0 is the rest wavelength of the given line, k is Boltzmann's constant, T is the temperature, and m is the mass of the atom. Setting $\xi_{\mathrm{micro}} = 0\,\mathrm{km/s}$, we end up with thermal broadening.

2.3 Stellar parameters for FGK stars - the EW method

2.3.1 Line list and atomic data

2.3.2 Measuring EW

2.3.3 Determining abundances with MOOG

Bibliography

Aerts, C., Christensen-Dalsgaard, J., and Kurtz, D. W.: 2010, *Asteroseismology*

Ammler-von Eiff, M., Santos, N. C., Sousa, S. G., Fernandes, J., Guillot, T., Israelian, G., Mayor, M., and Melo, C.: 2009, *A&A* **5**07, 523

Andreasen, D. T., Sousa, S. G., Delgado Mena, E., Santos, N. C., Tsantaki, M., Rojas-Ayala, B., and Neves, V.: 2016, *A&A* **5**85, A143

Andreasen, D. T., Sousa, S. G., Tsantaki, M., Teixeira, G. D. C., Mortier, A., Santos, N. C., Suárez-Andrés, L., Delgado Mena, E., and Ferreira, A. C. S.: 2017, *A&A* **5**85, A143

Artigau, É., Kouach, D., Donati, J.-F., Doyon, R., Delfosse, X., Baratchart, S., Lacombe, M., Moutou, C., Rabou, P., Parès, L. P., Micheau, Y., Thibault, S., Reshetov, V. A., Dubois, B., Hernandez, O., Vallée, P., Wang, S.-Y., Dolon, F., Pepe, F. A., Bouchy, F., Striebig, N., Hénault, F., Loop, D., Saddlemyer, L., Barrick, G., Vermeulen, T., Dupieux, M., Hébrard, G., Boisse, I., Martioli, E., Alencar, S. H. P., do Nascimento, J.-D., and Figueira, P.: 2014, in *Society of Photo-Optical Instrumentation Engineers (SPIE) Conference Series*, Vol. 9147 of *Society of Photo-Optical Instrumentation Engineers (SPIE) Conference Series*, p. 15

Baraffe, I., Homeier, D., Allard, F., and Chabrier, G.: 2015, *A&A* **5**77, A42

Bensby, T., Feltzing, S., and Oey, M. S.: 2014, *A&A* **5**62, A71

Blackwell, D. E. and Shallis, M. J.: 1977, *MNRAS* **1**80, 177

Boyajian, T. S., von Braun, K., van Belle, G., McAlister, H. A., ten Brummelaar, T. A., Kane, S. R., Muirhead, P. S., Jones, J., White, R., Schaefer, G., Ciardi, D., Henry, T., López-Morales, M., Ridgway, S., Gies, D., Jao, W.-C., Rojas-Ayala, B., Parks, J. R., Sturmann, L., Sturmann, J., Turner, N. H., Farrington, C., Goldfinger, P. J., and Berger, D. H.: 2012, *ApJ* **7**57, 112

Casagrande, L., Ramírez, I., Meléndez, J., Bessell, M., and Asplund, M.: 2010, *A&A* **5**12, A54

Conod, U., Blind, N., Wildi, F., and Pepe, F.: 2016, in *Society of Photo-Optical Instrumentation Engineers (SPIE) Conference Series*, Vol. 9909 of *Proceedings of the SPIE*, p. 990941

Delfosse, X., Donati, J.-F., Kouach, D., Hébrard, G., Doyon, R., Artigau, E., Bouchy, F., Boisse, I., Brun, A. S., Hennebelle, P., Widemann, T., Bouvier, J., Bonfils, X., Morin, J., Moutou, C., Pepe, F., Udry, S., do Nascimento, J.-D., Alencar, S. H. P., Castilho, B. V., Martioli, E., Wang, S. Y., Figueira, P., and Santos, N. C.: 2013, in L. Cambresy, F. Martins, E. Nuss, and A. Palacios (eds.), *SF2A-2013: Proceedings of the Annual meeting of the French Society of Astronomy and Astrophysics*, pp 497–508

Dotter, A., Chaboyer, B., Jevremović, D., Kostov, V., Baron, E., and Ferguson, J. W.: 2008, *ApJS* **1**78, 89

Follert, R., Dorn, R. J., Oliva, E., Lizon, J. L., Hatzes, A., Piskunov, N., Reiners, A., Seemann, U., Stempels, E., Heiter, U., Marquart, T., Lockhart, M., Anglada-Escude, G., Löwinger, T., Baade, D., Grunhut, J., Bristow, P., Klein, B., Jung, Y., Ives, D. J., Kerber, F., Pozna, E., Paufique, J., Kaeufl, H. U., Origlia, L., Valenti, E., Gojak, D., Hilker, M., Pasquini, L., Smette, A., and Smoker, J.: 2014, in *Society of Photo-Optical Instrumentation Engineers (SPIE) Conference Series*, Vol. 9147 of *Society of Photo-Optical Instrumentation Engineers (SPIE) Conference Series*, p. 19

Girardi, L., Bressan, A., Bertelli, G., and Chiosi, C.: 2000, *A&A Supp.* **1**41, 371

Gray, D. F.: 2005, *The Observation and Analysis of Stellar Photospheres, 3rd ed.*

Kippenhahn, R. and Weigert, A.: 1994, *Stellar Structure and Evolution*, Springer-Verlag

Kjeldsen, H. and Bedding, T. R.: 1995, *A&A* **2**93, 87

Kotani, T., Tamura, M., Suto, H., Nishikawa, J., Sato, B., Aoki, W., Usuda, T., Kurokawa, T., Kashiwagi, K., Nishiyama, S., Ikeda, Y., Hall, D. B., Hodapp, K. W., Hashimoto, J., Morino, J.-I., Okuyama, Y., Tanaka, Y., Suzuki, S., Inoue, S., Kwon, J., Suenaga, T., Oh, D., Baba, H., Narita, N., Kokubo, E., Hayano, Y., Izumiura, H., Kambe, E., Kudo, T., Kusakabe, N., Ikoma, M., Hori, Y., Omiya, M., Genda, H., Fukui, A., Fujii, Y., Guyon, O., Harakawa, H., Hayashi, M., Hidai, M., Hirano, T., Kuzuhara, M., Machida, M., Matsuo, T., Nagata, T., Onuki, H., Ogihara, M., Takami, H., Takato, N., Takahashi, Y. H., Tachinami, C., Terada, H., Kawahara, H., and Yamamuro, T.: 2014, in *Society of Photo-Optical Instrumentation Engineers (SPIE) Conference Series*, Vol. 9147 of *Society of Photo-Optical Instrumentation Engineers (SPIE) Conference Series*, p. 14

Lebzelter, T., Heiter, U., Abia, C., Eriksson, K., Ireland, M., Neilson, H., Nowotny, W., Maldonado, J., Merle, T., Peterson, R., Plez, B., Short, C. I., Wahlgren, G. M., Worley, C., Aringer, B., Bladh, S., de Laverny, P., Goswami, A., Mora, A., Norris, R. P., Recio-Blanco, A., Scholz, M., Thévenin, F., Tsuji, T., Kordopatis, G., Montesinos, B., and Wing, R. F.: 2012, *A&A* **547**, A108

Lindgren, S., Heiter, U., and Seifahrt, A.: 2016, *A&A* **586**, A100

Meléndez, J. and Barbuy, B.: 1999, *ApJS* **124**, 527

Mucciarelli, A., Pancino, E., Lovisi, L., Ferraro, F. R., and Lapenna, E.: 2013, *ApJ* **766**, 78

Önehag, A., Heiter, U., Gustafsson, B., Piskunov, N., Plez, B., and Reiners, A.: 2012, *A&A* **542**, A33

Origlia, L., Oliva, E., Baffa, C., Falcini, G., Giani, E., Massi, F., Montegriffo, P., Sanna, N., Scuderi, S., Sozzi, M., Tozzi, A., Carleo, I., Gratton, R., Ghinassi, F., and Lodi, M.: 2014, in *Society of Photo-Optical Instrumentation Engineers (SPIE) Conference Series*, Vol. 9147 of *Society of Photo-Optical Instrumentation Engineers (SPIE) Conference Series*, p. 1

Quirrenbach, A., Amado, P. J., Caballero, J. A., Mundt, R., Reiners, A., Ribas, I., Seifert, W., Abril, M., Aceituno, J., Alonso-Floriano, F. J., Ammler-von Eiff, M., Antona Jiménez, R., Anwand-Heerwart, H., Azzaro, M., Bauer, F., Barrado, D., Becerril, S., Béjar, V. J. S., Benítez, D., Berdiñas, Z. M., Cárdenas, M. C., Casal, E., Claret, A., Colomé, J., Cortés-Contreras, M., Czesla, S., Doellinger, M., Dreizler, S., Feiz, C., Fernández, M., Galadí, D., Gálvez-Ortiz, M. C., García-Piquer, A., García-Vargas, M. L., Garrido, R., Gesa, L., Gómez Galera, V., González Álvarez, E., González Hernández, J. I., Grözinger, U., Guàrdia, J., Guenther, E. W., de Guindos, E., Gutiérrez-Soto, J., Hagen, H.-J., Hatzes, A. P., Hauschildt, P. H., Helmling, J., Henning, T., Hermann, D., Hernández Castaño, L., Herrero, E., Hidalgo, D., Holgado, G., Huber, A., Huber, K. F., Jeffers, S., Joergens, V., de Juan, E., Kehr, M., Klein, R., Kürster, M., Lamert, A., Lalitha, S., Laun, W., Lemke, U., Lenzen, R., López del Fresno, M., López Martí, B., López-Santiago, J., Mall, U., Mandel, H., Martín, E. L., Martín-Ruiz, S., Martínez-Rodríguez, H., Marvin, C. J., Mathar, R. J., Mirabet, E., Montes, D., Morales Muñoz, R., Moya, A., Naranjo, V., Ofir, A., Oreiro, R., Pallé, E., Panduro, J., Passegger, V.-M., Pérez-Calpena, A., Pérez Medialdea, D., Perger, M., Pluto, M., Ramón, A., Rebolo, R., Redondo, P., Reffert, S., Reinhardt, S., Rhode, P., Rix, H.-W., Rodler, F., Rodríguez, E., Rodríguez-López, C., Rodríguez-Pérez, E., Rohloff, R.-R., Rosich, A., Sánchez-Blanco, E., Sánchez Carrasco, M. A., Sanz-Forcada, J., Sarmiento, L. F., Schäfer, S., Schiller, J., Schmidt, C., Schmitt, J. H. M. M., Solano, E., Stahl, O., Storz, C., Stürmer, J., Suárez, J. C., Ulbrich, R. G., Veredas, G., Wagner, K., Winkler, J., Zapatero Osorio, M. R., Zechmeister, M., Abellán de Paco, F. J., Anglada-Escudé, G., del Burgo, C., Klutsch, A., Lizon, J. L., López-Morales, M., Morales, J. C., Perryman, M. A. C., Tulloch, S. M., and Xu, W.: 2014, in *Society of Photo-Optical Instrumentation Engineers (SPIE) Conference Series*, Vol. 9147 of *Society of Photo-Optical Instrumentation Engineers (SPIE) Conference Series*, p. 1

Ramírez, I. and Meléndez, J.: 2005, *ApJ* **6**26, 446

Rayner, J., Bond, T., Bonnet, M., Jaffe, D., Muller, G., and Tokunaga, A.: 2012, in *Ground-based and Airborne Instrumentation for Astronomy IV*, Vol. 8446 of *Proceedings of the SPIE*, p. 84462C

Rayner, J., Tokunaga, A., Jaffe, D., Bonnet, M., Ching, G., Connelley, M., Kokubun, D., Lockhart, C., and Warmbier, E.: 2016, in *Society of Photo-Optical Instrumentation Engineers (SPIE) Conference Series*, Vol. 9908 of *Proceedings of the SPIE*, p. 990884

Recio-Blanco, A., Bijaoui, A., and de Laverny, P.: 2006, *MNRAS* **3**70, 141

Santos, N. C., Sousa, S. G., Mortier, A., Neves, V., Adibekyan, V., Tsantaki, M., Delgado Mena, E., Bonfils, X., Israelian, G., Mayor, M., and Udry, S.: 2013, *A&A* **5**56, A150

Sousa, S. G., Santos, N. C., Mayor, M., Udry, S., Casagrande, L., Israelian, G., Pepe, F., Queloz, D., and Monteiro, M. J. P. F. G.: 2008, *A&A* **4**87, 373

Torres, G., Andersen, J., and Giménez, A.: 2010, *Astronomy and Astrophysics Reviews* **1**8, 67

Torres, G., Fischer, D. A., Sozzetti, A., Buchhave, L. A., Winn, J. N., Holman, M. J., and Carter, J. A.: 2012, *ApJ* **7**57, 161

Torres, G., Winn, J. N., and Holman, M. J.: 2008, *ApJ* **6**77, 1324

Tsantaki, M., Sousa, S. G., Adibekyan, V. Z., Santos, N. C., Mortier, A., and Israelian, G.: 2013, *A&A* **5**55, A150

Tsantaki, M., Sousa, S. G., Santos, N. C., Montalto, M., Delgado-Mena, E., Mortier, A., Adibekyan, V., and Israelian, G.: 2014, *A&A* **5**70, A80

Valenti, J. A. and Fischer, D. A.: 2005, *ApJS* **1**59, 141